Contents list available at IJRED website

Int. Journal of Renewable Energy Development (IJRED)

Journal homepage: http://ejournal.undip.ac.id/index.php/ijred

Research Article

Post-Impact Characteristics of a Diesel-in-Water Emulsion Droplet on a Flat Surface Below the Leidenfrost Temperature

Ahmad Muneer El-Deen Faik[a1], Maathe A. Theeb[a], Yang Zhang[b]

[a] *Mechanical Engineering Department, College of Engineering, Mustansiriyah University, Baghdad, Iraq*

[b] *Mechanical Engineering Department, The University of Sheffield, Sheffield, UK*

ABSTRACT. Droplet impingement on solid surfaces takes place in a variety of industrial and environmental applications. However, there are still some areas that are not fully comprehended; emulsion droplet impact on a heated surface is one of these areas that require further comprehension. Hence, the present work represents an experimental exploration for spread characteristics of diesel-in-water (DW) emulsion droplet impacting a heated flat plate. Three different emulsions in which water concentration is set to 10%, 20%, and 30% of the overall emulsion content by volume have been tested in addition to the neat diesel. The temperature of the flat plate is varied over the range 20, 40, 60, and 80ºC respectively. Magnified high speed direct imaging and shadowgraphy have been used simultaneously for tracking droplet spread over the heated surface post impact. Droplet spread rate, maximum diameter, rebound height and velocity represent the main evaluated parameters. The results show that the maximum spread diameter is proportional while spread rate is inversely proportional to the increase in plate temperature for all diesel concentrations including the neat diesel. Whereas, droplet rebound height and velocity are found to be more responsive to the variation in diesel concentration than the variation in plate temperature, so they are both minimum in the case of neat diesel and are increasing by the decrease of diesel concentration in the emulsions.

Keywords: droplet impact, diesel, diesel-in-water emulsion, spread, Leidenfrost, heated flat plate

Article History: Received: 9th Sept 2020; Revised: 12th Dec 2020; Accepted: 31st Dec 2020; Available online: 2nd January 2021
How to Cite This Article: Faik, A.M. E. D., Theeb, M. A, and Zhang, Y. (2021) Post-Impact Characteristics of a Diesel-in-Water Emulsion Droplet on a Flat Surface below the Leidenfrost Temperature. *International Journal of Renewable Energy Development*, 10(2), 297-306.
https://doi.org/10.14710/ijred.2021.34036

1. Introduction

Droplet impingement on solid surfaces takes place in a variety of industrial and environmental applications. These include – but not limited to – rain drops, spray cooling, spray painting, inkjet printing, and fuel injection (Rueda Villegas *et al.,* 2017). Besides, droplet response to its impact on a solid surface – in its own – grabs the interests as a complex hydrodynamic phenomenon (Sen *et al.*, 2020). This interaction depends on the conditions of that surface, such as roughness (Chakaneh *et al.,* 2019; Zhang *et al.*, 2018), texture (Alizadeh *et al.,* 2012; Moon *et al.*, 2016; Qi & Weisensee, 2020; Wang *et al.,* 2017), wettability (Li & Duan, 2019; Qi & Weisensee, 2020; Raman *et al.,* 2016), and inclination (Jin *et al.*, 2015, 2016; Li & Duan, 2019). Therefore, the droplet may spread, rebound, or splash away from the surface according to these physical conditions (Dunand *et al.,* 2013). One of these conditions that have a strong influence on the droplet-surface interaction is the surface temperature (Jowkar & Morad, 2019). (Jowkar & Morad, 2019) stated that droplet rebound and secondary atomization post-impact to a solid heated surface are determined by the surface temperature and Weber number. Weber number is defined as the ratio between the inertial force of the droplet and the cohesive force of the liquid. At low Weber number, the kinetic energy of the droplet is relatively small. This in turn, lets the droplet to spread, recede, and then rebound from the surface post-impact. Whereas, at high Weber number, the kinetic energy of the droplet is high enough to initiate breakup (Jowkar & Morad, 2019). (Alizadeh *et al.*, 2012) found that the surface temperature has a strong effect on the droplet dynamics post-impact on a heated surface, and recommended further investigations on this effect on variable surfaces. This is the same recommendation of (Gayatri *et al.,* 2015), however the latter researchers focused on the investigation of the effect of Leidenfrost temperature on the droplet dynamics. From these studies and much other more, it can be found that further comprehension of the effect of surface temperature on the droplet dynamics post-impact is indispensable. Hence, studying this effect would be the scope of the present work.

Diesel-water emulsions on the other hand represent one of the potential long term solutions to the harmful environmental impact of the diesel fuel exhaust emissions (Crookes *et al.,* 1997; Faik & Zhang, 2018; Faik & Zhang, 2020). Emulsification is the process of mixing immiscible liquids with the help of an agent called as the emulsifier (or surfactant). For diesel-in-water emulsions, diesel is the dispersed phase and water is the continuous phase,

[1] Corresponding author: a.faik@uomustansiriyah.edu.iq

whereas for the water-in-diesel emulsions, water is the dispersed phase and diesel is the continuous phase (Leal-Calderon *et al.*, 2007). The emulsifier is used in the emulsification process to form a protective strong film layer that helps inhibit phase separation between the continuous and dispersed phases. The type of emulsifier is defined by the type of emulsion. Hydrophilic emulsifiers are usually used for oil-in-water emulsions, with Hydrophile-Lipophile Balance (HLB) number ranging $11 \leq HLB \leq 20$, while the lipophilic emulsifiers are usually used for water-in-oil emulsions. The HLB number for the latter emulsifiers ranges $0 < HLB \leq 9$ (Mollet & Grubenmann, 2001). The behaviour of fuel emulsions during combustion and associated processes such as atomization, nucleation, and micro-explosion, is the focus of a great majority of research work (Faik & Zhang, 2018). However, the intricacy of the emulsified fuel combustion, in addition to the variable nature of the engine and environmental conditions within which the fuel is working makes the analysis a bit complicated and harsh work to be accomplished (Vellaiyan and Amirthagadeswaran, 2016). Consequently, further research is required for more in-depth understanding and better utilization of the fuel emulsions in combustion applications. Emulsion droplet impact on a heated surface is one of these areas that have been and being investigated. (Cen *et al.,* 2019) studied the micro-explosion of water-in-diesel emulsion droplet during its impact on a heated surface and found a strong relation between droplet micro-explosion and the temperature of the surface. The same is found by (Ashikhmin *et al.*, 2020) for biodiesel-in-water emulsion droplets impinging hot surfaces. (Tanimoto & Shinjo, 2019) on the other hand found that a sufficient amount of puffing generated by the emulsion droplet may cause droplet bouncing and detachment from the heated surface. This emphasizes a vital point that is the behaviour of the emulsion droplet post-impacting a heated surface is different from that of the neat liquid droplet. This in turn, has its effect on the droplet – and then spray – atomization and the overall combustion behaviour of the emulsion-based fuel. Therefore, the previously set scope of work is further narrowed to the post-impact behaviour of the diesel-in-water emulsion droplet on a heated surface. This scope is of practical importance in the diesel engines and has been investigated by a number of research articles such as those shown in (Ashikhmin *et al.*, 2020; Cen *et al.*, 2019; Tanimoto & Shinjo, 2019). The essential part in such problems is liquid boiling and the so-called Leidenfrost phenomenon, which is defined as liquid levitation due to rapid vapour formation for the liquid being in contact with a solid surface at a temperature higher than that of the liquid boiling point (Rueda Villegas *et al*., 2017). Hence, the majority of the research work conducted for emulsion droplet interaction with a heated surface is dedicated to temperatures above the Leidenfrost temperature. However, there is another side of the problem that is the emulsion droplet impingement on the piston during the early period of engine operation, i.e. engine cold start and warm up period. Engine cold start period is defined as the interval of time within which the temperature of all engine components equals – or close – to the environmental temperature (Bielaczyc *et al.*, 2014), i.e. below the boiling point of the fuel or in other words, below the Leidenfrost point. Despite its shortage in relation to the overall engine working time, the importance of the cold start period comes from the fact that about 80-90% of the total harmful engine emissions are produced during this period (Samuel & Valan, 2014). This problem has been the scope of a considerable number of research articles such as (Crookes *et al.*, 1997; Faik, 2018; Shi *et al.*, 2019; Wang *et al.*, 2016; Yang *et al.*, 2020). However, all of these articles have dealt with either neat diesel or diesel blends as working fuels rather than diesel-based emulsions, and that to the authors' best knowledge, the problem of diesel-emulsion behaviour during engine cold start conditions has not been covered. Consequently, the rest of the present work would be dedicated to investigate the post-impact dynamics of the diesel-in-water emulsion droplet on a heated surface below the Leidenfrost temperature analogues to engine cold start conditions. This would be performed experimentally in-lab using high speed imaging and off-lab using digital image processing for temporal tracking of the associated physical processes. Finally, it is worth to mention that diesel-in-water emulsion is investigated in the present work rather than the water-in-diesel emulsion due to two reasons, the first is that the data available for the former is less compared to that of the latter, and the second is that there is an evidence that the stability of the diesel-in-water emulsions is found to be higher (Ithnin *et al.*, 2015; Wamankar *et al.*, 2015).

2. Materials and Methods

2.1 Emulsion Preparation

Three diesel-in-water emulsions are prepared in the present work. In these emulsions, water quantity is set to 10%, 20%, and 30% of the total emulsion volume, and the remaining 90%, 80%, and 70% of the mixture represent the corresponding neat diesel portions respectively. Polysorbate 80 (HLB = 15) emulsifying agent is used for increasing emulsions stability. The emulsions have been prepared in-lab prior to experiments. The method used for emulsion preparation is that followed and described by both (Califano *et al.,* 2014) and (Jackson & Avedisian, 1998), and it is as follows: for each emulsion, a specified quantity (< 1% of the total mixture volume) of the Polysorbate 80 is added to the set quantity of water with continuous stirring for better solubility. The corresponding quantity of diesel is then added gradually to the mixture. The mixture is stirred using a 20000 rpm hand blender for about 5 minutes, after which a homogeneous milky white liquid is obtained. This implies a coarse macro-emulsion with disperse phase particles (Mollet & Grubenmann, 2001). The above steps have been followed for producing all emulsion samples implemented in the present work and for all proportions. Hence, for easier interpretation, the prepared emulsions are termed as DW10, DW20, and DW30 for referring to the emulsions of 10% water + 90% diesel, 20% water + 80% diesel, and 30% water + 70% diesel respectively. Finally, it should be emphasized that for accuracy purposes, and to eliminate the probability of emulsion phase separation and its effect on the results, a new emulsion sample is prepared for every test run, although no visible changes are observed on the prepared samples during the tests.

2.2 Experimental Setup and Procedures

Fig 1 (a) shows the experimental setup used in the present work. A micro-fine syringe with hypodermic (0.33mm diameter by 12.7mm length) needle is used for generating and ejecting the droplet. The syringe is attached to a lab-stand on a 100 cm height from the hot flat plate. The plate is a 20 cm diameter aluminium plate fixed on-top of a 1500 Watt, 21.5 by 21.5 by 7cm) domestic electric heater. A -50 to 900ºC Douself LCD non-contact IR Infrared thermometer has been used for plate temperature measurement. Four values of the plate temperature are used in experiments namely 20, 40, 60, and 80ºC. A Photron SA4 high speed camera equipped with a Nikon AF Micro NIKKOR 60mm f/2.8D lens and a 55mm macro extension tube set is used for tracking the droplet subsequent impinging the flat plate. The camera is set to 3000 frames per second imaging rate, 1/5000 s shutter speed, and 1024 by 1024 image resolution. With this setup, the area covered by camera is 244 mm width by 244 mm height. An IDT 19-LED, 48-Volt, 200 Watt, high intensity illuminator has been used to provide the required light on-top of the plate. This imaging setup is suitable for tracking droplet spread and diameter variation post-impact, nonetheless it is not suitable for tracking the rebound, disintegration, and side dynamics taking place during droplet spread. Accordingly, for tracking such dynamics, another imaging setup based on z-type shadowgraphy is used as shown in Fig 1(b).

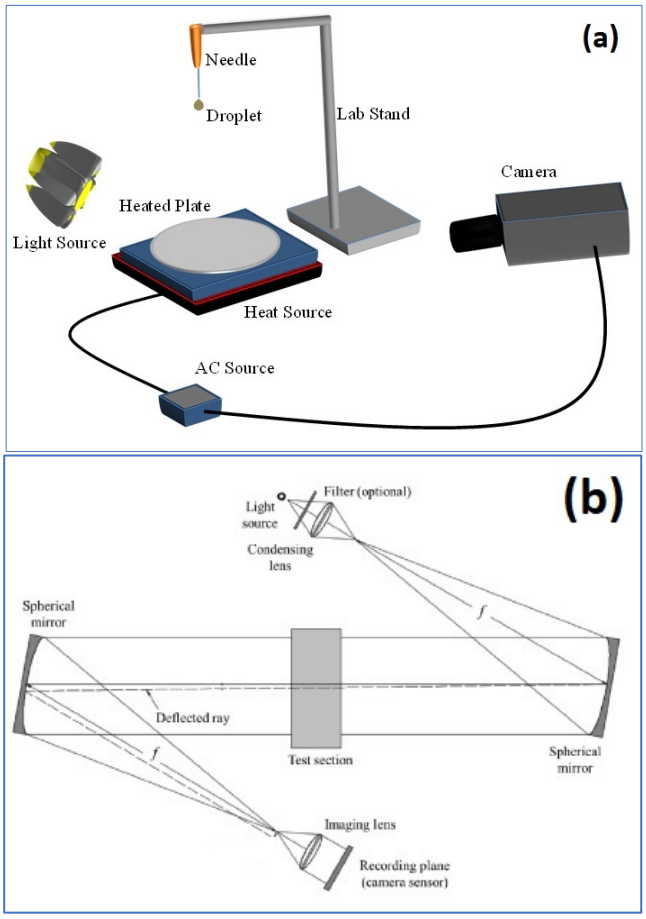

Fig 1. Experimental setup with (a) direct imaging, and (b) shadowgraph imaging.

This setup consists of 2-parabolic 30.48cm diameter mirrors and a 150 Watt halogen light source with 2-condensing lenses, one next to the light source and the other before the camera. The camera has also been set to 3000 frames per second imaging rate, and 1/25000s shutter speed, and 1024 by 1024 image resolution. The shutter speed is different from that of the direct imaging in order to adjust the light intensity in the image. As soon as the plate temperature reaches the set point, the droplet is ejected from the syringe (image recording starts at this moment) until the droplet settles on the flat plate and no visible size variation is detected (at this point recording terminates). Even though the starting time of the present investigation is set to be at the moment the droplet hits the plate. The images acquired by camera are stored in the (JPG) format and post-processed using a specially written Matlab algorithm. The post processing work includes reading and cropping the raw image, image enhancement, segmentation and morphological operations, feature extraction, and data saving. The extracted features are the instantaneous droplet equivalent diameter, projected area and circumference, maximum spread diameter, spread rate and velocity. Further details on image processing work carried out for extracting the flow features can be found in (Faik, 2017). The average droplet diameter is evaluated by image processing and is found to be 2±0.1 mm for all the generated droplets. The (±0.1) represents the standard deviation of the results, which indicate a relatively high repeatability of the droplet diameter using the above explained droplet generation technique.

3. Results and Discussion

Fig 2 shows the temporal variation of DW10 droplet shape on a 20°C plate as it is tracked by the direct imaging setup. The time difference between each two successive images is (333 µs). The time is assumed to start from the moment the droplet makes the first contact with the surface of the plate (left image of the first raw of Fig 2), whereas the end time is assumed as the time when the droplet reaches its maximum spread area (right image of the last raw of Fig 2). This is decided by image processing, where the instantaneous droplet size variation becomes negligibly too small to be evaluated. Keeping in mind that it is aimed to study the behaviour of the droplet spread just post-impacting the solid surface to mimic spray impingement with engine piston, therefore, the effect of droplet settling on the solid surface is beyond the scope of the present work. Hence, Fig 2 shows a tracking of the full post-impact behaviour experienced by the droplet until it reaches its maximum spreading area. Firstly, the droplet is spherical (or precisely semi-spherical), then it spreads horizontally due to the kinetic energy produced by droplet impingement on the solid surface. The instantaneous and average values of the droplet shape and diameter during spread are evaluated for all the fuels under investigation and for all plate temperature values, and will be discussed later. It can be noticed for the figure that during its spread, the droplet takes an elliptical – rather than circular – shape due to the instability waves generated by impact (Borisov *et al*., 1981). This is in agreement with the finding of (Gayatri *et al*., 2015) for 2 mL and 3 mL size droplets at the Leidenfrost point.

However, direct imaging does not give a full description of what is happening to the droplet from the moment of the impact, therefore shadowgraph imaging has been used for more in-depth tracking of the processes associated to droplet impact. Fig 3 shows a sample of these shadowgraph images for a droplet of the same mixture of that in Fig 2 (i.e. DW10). The time difference between each two successive images is also (333 μs). As it is shown in the figure, the droplet experiences a form of disintegration into smaller size sub-droplets just after its impingement on the plate, this disintegration could not be sensed by the former direct imaging method.

This droplet breakup or disintegration has been reported by a number of studies (Gayatri *et al.*, 2015; Sen *et al.,* 2020) and is usually termed as secondary atomization. The distance travelled by the sub-droplets generated by the disintegration of the original droplet is evaluated in addition to the velocity and angle, and would be discussed later.

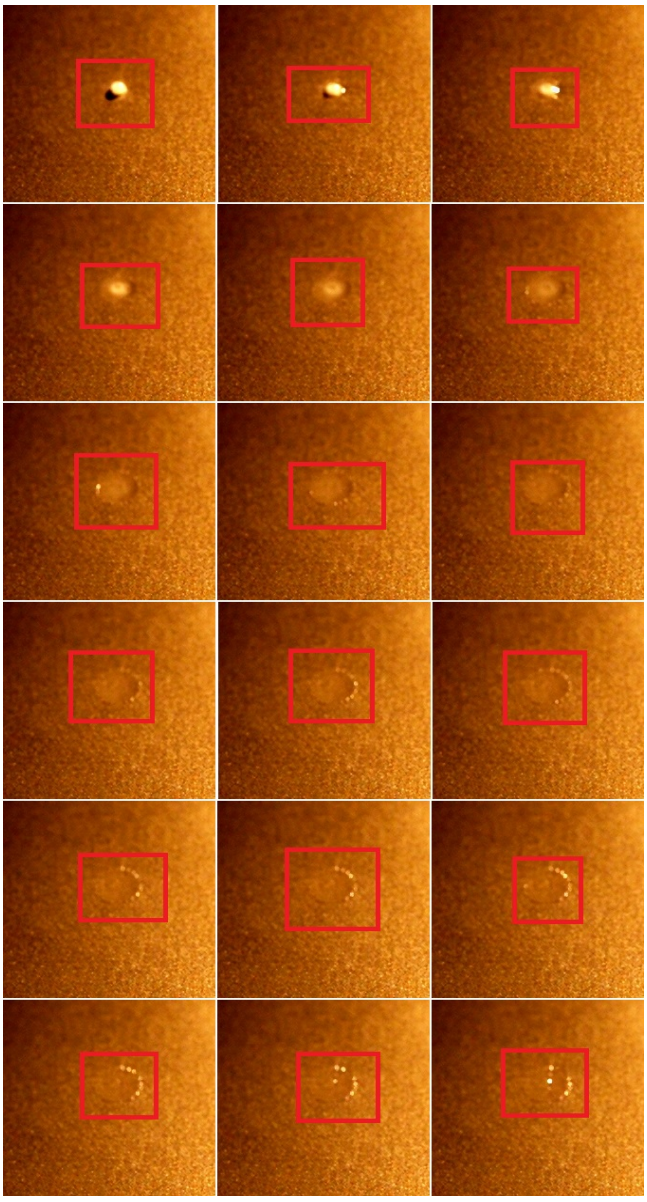

Fig 2. Sequential tracking of DW10 droplet on a 20°C plate.

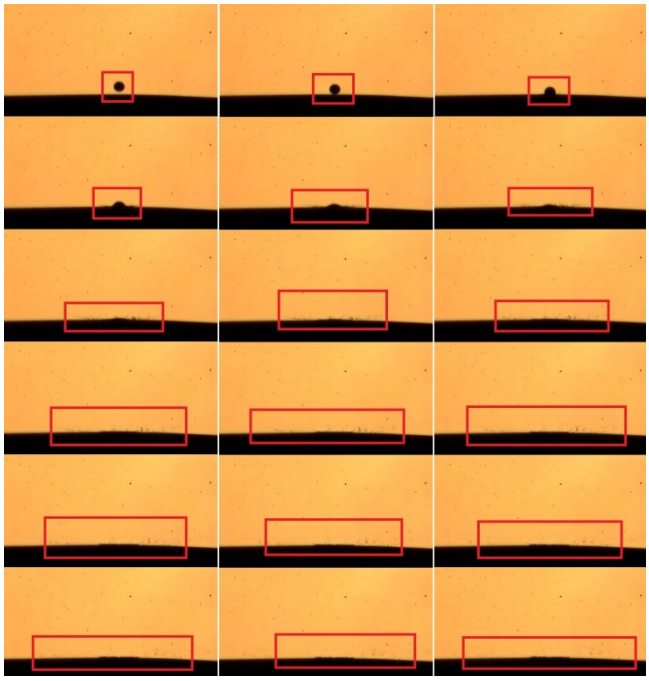

Fig 3. Shadowgraph imaging of the post-impact sequence of a DW10 droplet on a 20°C plate.

Fig 4 shows the effect of plate surface temperature on the temporal variation of the normalized droplet diameter (D/D_0) post-impact for neat diesel and the diesel-in-water emulsions DW10, DW20, and DW30 respectively. The time has been normalized by the total time required by the droplet to reach its maximum diameter, thence, the time presented in the figure is the percentage of the overall time (from 0 to 1). From Fig 4 it can be seen that the maximum diameter in the emulsion droplets DW10, DW20, and DW30 is proportional to the surface temperature of the flat plate. Nevertheless, this proportionality is not so obvious in the case of neat diesel fuel droplet. Although there are no published data for the emulsions, those for the neat diesel fuel show a consistency with those published in literature such as the results demonstrated by (Rueda Villegas *et al.,* 2017). It can be shown also that there are two distinct regions in the size variation of the droplet for all the fuels under investigation including neat diesel fuel. These regions are separated by a period of no – or slow – size variation as bounded by the red circles in the graphs of Fig 4. This division in the droplet size growth can be explained in light of the description given by Li et al., (Li *et al.*, 2017) for the three regions of water droplet size variation upon impact on a heated surface. They termed these regions as spread region, receding region, and oscillation region respectively. With the first region, droplet size increases and its height decreases due to the kinetic energy as discussed above, whereas, for the second region, droplet size increase is too small, while its centres thickness increases. And lastly, for the third region, droplet size increase continues similar to the first region. This description is almost in agreement with the behaviours presented in Fig 4, although droplet centre thickness increase has not been visualized, because of the view angle of the imaging setup which is directed on-top the plate. Furthermore, it can be noticed from Fig 4 that for the same

plate surface temperature, the value of the maximum droplet size shows proportionality with the value of the water content in the mixture, i.e. increasing the water content in the mixture increases the maximum diameter of the droplet for the same surface temperature. This trend is in agreement with the findings of (Ashikhmin *et al.,* 2020) for diesel/biodiesel emulsion with water (water concentration 10-20%) at high surface temperatures (above the Leidenfrost point). However, (Qiao & Chandra, 1996) found that the maximum spread diameter of the water droplet is much lower than that of the n-heptane droplet for the same temperature, and claimed that this difference is due to the high surface tension of water compared to that of n-heptane, so it prevents water spread. Nonetheless, this explanation may be related to the behaviour of the neat liquids, and in the case of mixtures, most likely, the scenario would be different. This is shown by (Sen *et al.,* 2020) for binary-water-mixture droplet behaviour post-impact compared to the behaviour of neat water droplet.

Fig 5 shows the effect of plate surface temperature on the temporal variation of the normalized droplet spread rate for neat diesel, DW10, DW20, and DW30 emulsion droplets respectively. The spread rate is in (1/s) units since it is divided by the droplet impact diameter to eliminate its effect on the results, while the time is normalized by the total spread time as emphasized earlier. From Figure 5, it can be seen that the droplet spread rate is fluctuating with time for all the fuels, and that this fluctuation takes the sinusoidal form as shown by the trend-lines added for each graph. Additionally, it can be seen from the figure that for all the fuels, the spread rate is increasing for the first 30% of the time until reaching a maximum value, and then it starts to decrease for the rest of the time. This is in agreement with the period of time specified by (Qi & Weisensee, 2020) through which the maximum heat transferred from the hot surface to the droplet upon impact is being maximum.

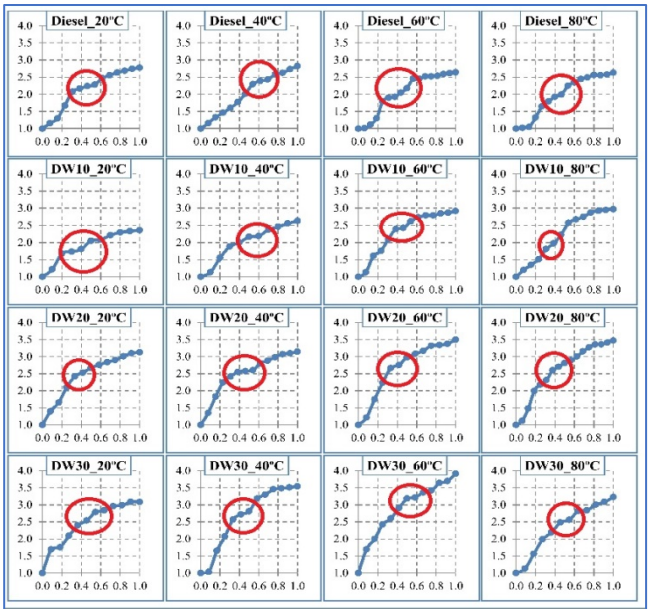

Fig 4. The effect of plate temperature on the normalized droplet diameter variation (y-axis) with normalized spread time (x-axis) for diesel and emulsions.

This portion of time has been termed as the spreading period, whereas the rest 70% has been termed as the receding period. Although for the emulsion droplets, the droplet experiences a second increase in the spread rate at the final 20% of the total time. This is attributed to nucleation inside the emulsion droplet compared to the neat diesel droplet that does not experience nucleation (Faik, 2017). Again it can be shown that the neat diesel droplet is irresponsive to the change in plate surface temperature, whereas a form of proportionality can be sensed for the emulsion droplets. This proportionality can also be seen for the comparison of water content for the same plate surface temperature. Therefore, it can be inferred that changing either the water content or the plate surface temperature has its direct effect on the dynamics of the diesel-in-water emulsion droplets. Whereas, for the neat diesel fuel, the scenario is slightly different, probably because the plate surface temperature values are far from the diesel boiling point, therefore, no considerable variation with temperature are noticed for the neat diesel fuel droplet during spread. This in turn, makes the analysis for the diesel-in-water emulsions more valuable, since its behaviours are slightly different from those of the neat diesel fuel.

Fig 6 shows the effect of plate surface temperature on the average values of total spreading time, maximum spread diameter, spreading velocity, and spread rate respectively of both neat diesel, DW10, DW20, and DW30 fuel droplets. The post-impact average total spreading time (upper left graph) is shown to be proportional to the variation in plate surface temperature for all the fuel under investigation. Firstly, it should be emphasized that although the analogy is for droplet impingement on the piston of the internal combustion engine, in which the time available for the spray – and droplets – is too short, but it is still possible for the droplet to spread within the presented time since the injection time is in the order of (1.5-10 ms) (Pulkrabek, 1997) which is within the range shown in Fig 6 even though the real droplet in the engine spray is much smaller than that produced in-lab.

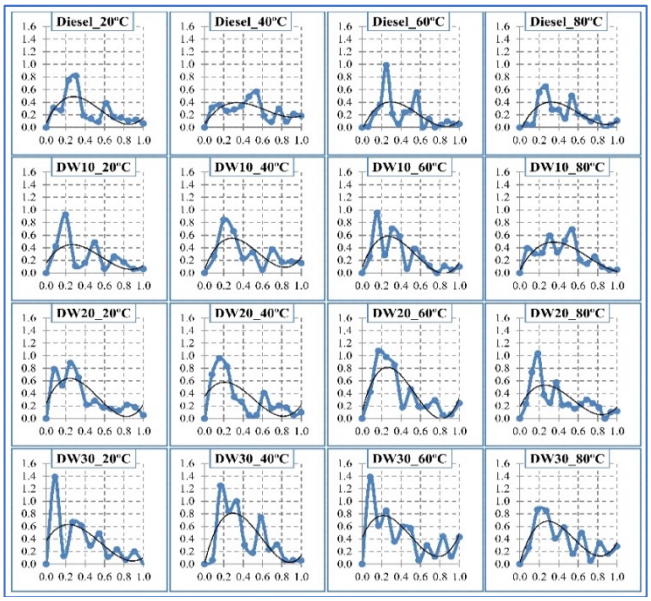

Fig 5. The effect of plate temperature on the variation of the droplet spread rate (*10^3) (y-axis) with normalized time (x-axis) for diesel and emulsions.

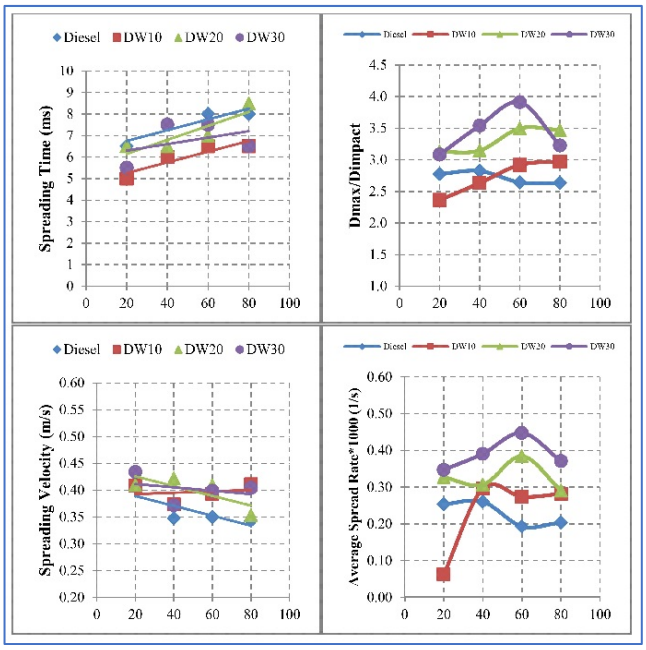

Fig 6. The effect of plate temperature (x-axis) on the variation of droplet spread time (upper left), maximum diameter (upper right), spread velocity (lower left), and spread rate (lower right).

It can be seen from the same graph that for the DW10, Dw20, and DW30 fuel droplet emulsions, and for the same surface temperature, the total spreading time is almost proportional to the water content in the emulsion, which is in agreement with the previous finding for the droplet maximum spreading diameter. However, the neat diesel droplets showed a higher spreading time compared to the corresponding emulsion droplets for the same plate surface temperature. Again, this may be attributed to the difference in behaviour between the neat liquids and their binary mixtures, especially emulsions. The heat transferred from the hot surface to the droplet causes boiling and evaporation of water in the emulsion. This evaporation leads to bubble formation inside the droplet, this in turn enhances droplet size increase, i.e. spread (Cen *et al.*, 2019). Consequently, droplet spread time is decreased in the case of emulsions. However, bubble generation inside the droplet does not take place in the case of neat diesel fuel, resulting in increasing the spread time. The same behaviours are shown for the upper right graph of Fig 6 which presents the response of the average maximum spread diameter of the fuels under investigation to the variation in plate surface temperature. However, the neat diesel fuel droplets gave a kind of inversely proportional response to the plate surface temperature.

The repeatability of the results has been evaluated by the standard deviation (STD) of the results for all the calculated samples. STD in the case of maximum spread diameter is evaluated for each fuel at every temperature, and its maximum values are 0.62, 0.72, 0.87, and 0.93 for the neat diesel, DW10, DW20, and DW30 emulsions, respectively. These values are about 10-20% of the spread diameter values, indicating a relatively acceptable repeatability. The average droplet spread velocity (lower left graph of Fig 6), on the other hand, shows a different behaviour, where an inverse response of the average spread velocity is obtained for all the fuels under investigation including the neat diesel. The spread velocity is evaluated by evaluating the axial distance travelled by the liquid on the surface for each image and dividing it by the interval of time required, and then the average value of these magnitudes is evaluated for each sample droplet. It can be seen from the graph that the values of the spreading velocity are too close for all the fuels, indicating a less influence of the water content on the spread velocity compared to the plate surface temperature. This influence of water content is more obvious in the spread rate (lower right graph of Fig 6), even though the neat diesel droplets show a slightly different response to the variation in plate surface temperature compared to those of the emulsion droplets. Additionally, at surface temperature (80°C), the behaviour is slightly different. This could be attributed to the fact that the later temperature is closer to the boiling point of water compared to other temperature values. This in turn increases the chances of nucleation and water boiling inside the emulsion droplet, and subsequently decreases its effect on the droplet geometry. However, the maximum STD values in this case are found to be (0.25, 0.29, 0.36, and 0.4) for the neat diesel, DW10, DW20, and DW30 fuels respectively, which indicate a high diversity in the results. Furthermore, post-impacting the heated surface, it is noted that droplet spread was not symmetric. The droplet took the shape of an ellipse rather than a full circle as shown in Fig 2. Therefore, the equivalent diameter has been evaluated rather than the true diameter for evaluating the droplet diameter during spread. A number of techniques are available in literature for evaluating the equivalent diameter, though; the one implemented in the present work is the square root of the projected area. This method is based on evaluating the projected area of the droplet using image processing in Matlab. This area is equivalent to the area of a uniform circle whose diameter is (d), from which the diameter is evaluated. Further details on the equivalent diameter evaluation methods and precision of each method can be found in (Faik, 2017). For that reason, and to highlight the elliptical configuration of the droplet post-impact, the average values of the main features of the ellipse are evaluated and presented in Fig 7. These features include the major diameter, minor diameter, aspect ratio (major/minor), and instantaneous diameter. The instantaneous major and minor diameter of the droplet post impact are easily evaluated through image processing by Matlab, The major diameter is longest diameter in the ellipse formed by the droplet, whereas the minor diameter represents the shortest diameter. Both of these diameters give an indication of the degree of deformation of the droplet by comparing its elliptical shape to the full circle configuration. This is evaluated by the aspect ratio; that is the ratio between the major and minor diameters of the ellipse (Tanaka *et al.*, 2011). If the ratio equals to 1, then the ellipse is a full circle, otherwise the shape is elliptical. The first – upper left – graph of Fig 7 shows the droplet average major diameter variation with plate surface temperature for all the fuels under investigation. From the graph, it can be inferred that the average droplet major diameter is inversely proportional to the plate surface temperature in the case of neat diesel droplet,

whereas those of the emulsion droplets are slightly different in behaviour with increasing trend in the first temperature values until 60°C, then they are decreasing for the last temperature, i.e. 80°C. Again, this is attributed to the same reason mentioned above for the 80°C being closer to water boiling point compared to other temperature values. This results in increasing the chances of nucleation and water boiling inside the emulsion droplet, and subsequently decreases its effect on the droplet geometry.

Additionally, for every plate temperature value, the values of the major diameter for all the fuels are close to each other, indicating minor influence of the water content on the major diameter. The maximum STD values for this case are shown to be 0.72, 0.80, 0.93, and 0.85 for the neat diesel, DW10, DW20, and DW30 fuels respectively. This indicates an acceptable level of repeatability. The upper right graph of Fig 7 shows the response of the average droplet minor diameter of the fuels under investigation to the variation in plate surface temperature.

From Fig 7, it can be inferred that the droplet minor diameter is almost increasing with the increase in plate surface temperature in the case of emulsion droplets, whereas the neat diesel droplets have shown a more irresponsive behaviour regarding the droplet minor diameter. Moreover, for the same plate surface temperature, it can be shown that the droplet minor diameter values are more susceptible to the variation in water content of the mixture, where increasing the water content increases the value of the droplet minor diameter for all the fuels under investigation. Nonetheless, the DW10 droplets are closer in the value to the neat diesel droplets than the DW20 and DW30 which are close to each other as well. The same trends are shown in the case of the average instantaneous diameter (lower right graph of Fig 7).

The aspect ratio – lower left – graph of Fig 7 on the other hand, shows a similarly proportional behaviour with respect to the plate surface temperature. However, relatively high values of the neat diesel droplet are obtained compared to the emulsion droplets which have slightly comparable lower values. Although, at plate surface temperature 80°C, the aspect ratio of the neat diesel fuel droplet converge to those of the emulsion droplets. In addition, an almost inverse proportionality can be perceived between the variation in water content and the resulting aspect ratio.

Till now, the discussions were dedicated to the results obtained from the direct imaging setup, whereas shadowgraph imaging has also been implemented in the present work as discussed earlier. Hence, the results obtained from the shadowgraph images are analysed and the results are shown in Fig 8. Shadowgraph imaging was devoted for tracking the secondary atomization of the droplets post-impact the heated surface, in addition to comparing the rebound of the sub-droplets with respect to the original droplet. Therefore, Fig 8 shows the effect of plate surface temperature on average values of the maximum spread axial distance, maximum rebound height, rebound velocity, and spread angle respectively of the sub-droplets generated by original droplet disintegration (or secondary atomization) for the neat diesel, DW10, DW20, and DW30 emulsions. The first (upper left) graph of the figure shows the variation of maximum spread axial distance travelled by the sub-droplets with respect to the plate surface temperature. The maximum spread axial distance is selected for investigating the effective area of the droplet upon impact, and is normalized by the diameter of the original droplet upon impact (D_0) to eliminate its effect on the results. The maximum axial travelled distance is evaluated by digital processing of the shadowgraph images for the sub-droplets generated just after droplet impact on the heated surface.

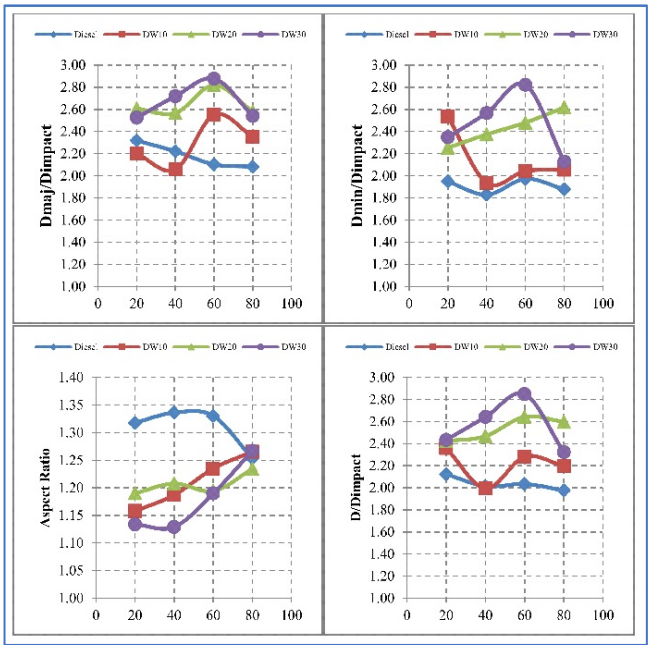

Fig 7. The effect of plate temperature (x-axis) on the variation of average values of normalized droplet major diameter, normalized droplet minor diameter, aspect ratio, and instantaneous diameter respectively.

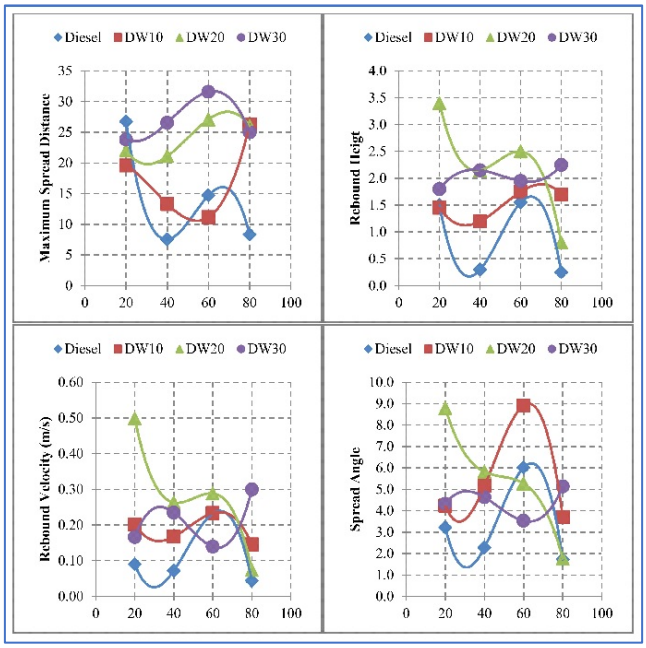

Fig 8. The effect of plate temperature on the normalized values of maximum spread distance, rebound height, rebound velocity, and spread angle respectively.

This processing is based on evaluating the area covered by these sub-droplets with respect to the total area of the image, then extracting the maximum horizontal length of this area. From the graph, it can be seen that the axial distance travelled by the sub-droplets may reach about (20-30) times the diameter of the original droplet for all fuels. This in fact is a huge number if compared with the maximum spread diameter of the original droplet shown in Fig 6 which reaches 4 in its highest value. This alone is a good compromise for supporting the use of shadowgraph imaging in droplet impingement investigations. The maximum STD values for the spread distance for each fuel are 8, 6.8, 2.9, and 3.4, respectively, indicating a relatively acceptable degree of repeatability, especially for the emulsion droplets. Additionally, it can be inferred from the graph that the effect of water concentration in the mixture is effective in deciding the behaviour of the sub-droplets with respect to temperature. This is shown on the decreasing behaviour of the neat diesel and DW10 sub-droplets compared to the increasing behaviour of the DW20 and DW30 sub-droplets. The same behaviours are obtained for the sub-droplets maximum vertical rebound from the surface (upper right graph of Fig 8). This rebound has also been normalized by the impact diameter of the original droplets. The maximum STD values for the rebound height for neat diesel, DW10, DW20, and DW3 fuels are 0.7, 0.2, 1, and 0.2, respectively. The sub-droplet rebound velocity (lower left graph of Fig 8) has also been evaluated, its values are comparable to those evaluated by Castanet et al., (Castanet *et al.,* 2013) who has also implemented shadowgraph imaging for sub-droplet tracking. The effect of water content on the rebound velocity is relatively more obvious, where increasing water content in the fuel increases the rebound velocity of the sub-droplets for the same plate surface temperature. The maximum STD values for the rebound velocity for neat diesel, DW10, DW20, and DW3 fuels are 0.08, 0.04, 0.17, and 0.07, respectively. Again, a high degree of repeatability is obtained from these values. The angle created by the path of the sub-droplets with the horizontal axis is evaluated and shown in the lower right graph of Fig 8. This angle – termed as the spread angle – is ranging as (2-10). From the graph, the same distinction between neat diesel and DW10 on one side and the DW20 and DW30 on the other can be concluded. Where, the spread angle created by the former group is found to be proportional to the variation in plate surface temperature, while the angle of the latter group is inversely proportional. The maximum STD values for the spread angle for neat diesel, DW10, Dw20, and DW3 fuels are 1.9, 2.3, 2.8, and 0.7, respectively.

4. Conclusion

In this work an experimental evaluation of the effect of plate surface temperature on the post-impact behavior of the neat diesel and diesel-in-water emulsion droplets. Three different values of water concentration are used in the emulsions; namely 10%, 20%, and 30% of the overall emulsion volume. The main points concluded from this work are as follows. Post-impacting the heated surface, droplet spread is not symmetric. The droplet took the shape of an ellipse rather than a full circle. The maximum diameter in the emulsion droplets is shown to be proportional to the surface temperature of the flat plate. Nevertheless, this proportionality is not so obvious in the case of neat diesel fuel droplet. Additionally, two distinct regions in the size variation of the droplet for all the fuels under investigation are noticed. These regions are separated by a period of no – or slow – size variation. Furthermore, for the same plate surface temperature, the value of the maximum droplet size shows proportionality with the value of the water content in the mixture. The droplet spread rate, on the other hand, is shown to be fluctuating with time for all the fuels, and this fluctuation takes the sinusoidal form. Additionally, the spread rate is increasing for the first 30% of the time until reaching a maximum value, and then it starts to decrease for the rest of the time. Moreover, the post-impact average total spreading time is proportional to the variation in plate surface temperature for all the fuels under investigation.

It is found also that for the emulsion fuel droplets, and for the same surface temperature, the total spreading time is almost proportional to the water content in the emulsion. The same behavior is shown for the average maximum spread diameter. However, the average droplet spread velocity is inversely proportional to the plate surface temperature for all the fuels under investigation. The values of the spreading velocity are too close for all the fuels, indicating a less influence of the water content on the spread velocity compared to the plate surface temperature. The average droplet major diameter on the other hand, is found to be inversely proportional to the plate surface temperature in the case of neat diesel droplet, whereas those of the emulsion droplets are slightly different in behavior with increasing trend in the first temperature values until (60°C), then they are decreasing for the last temperature, i.e. (80°C). A minor influence of the water content on the major diameter is obtained. However, the droplet minor diameter is almost increasing with the increase in plate surface temperature in the case of emulsion droplets, whereas the neat diesel droplets have shown a more irresponsive behavior regarding the droplet minor diameter.

Besides, the maximum spread axial distance travelled by the sub-droplets may reach about (20-30) times the diameter of the original droplet for all fuels. This in fact is a huge number if compared with the maximum spread diameter of the original droplet which reaches (4) in its highest value. Water concentration in the mixture is found to be effective in deciding the behavior of the sub-droplets with respect to temperature. The same behaviors are obtained for the sub-droplets maximum vertical rebound from the surface. Increasing water content in the fuel increases the rebound velocity of the sub-droplets for the same plate surface temperature.

Acknowledgments

The experimental work has been carried out in the combustion diagnosis lab in Department of Mechanical Engineering, The University of Sheffield, UK. Additionally, the authors would like to acknowledge the support received from the staff of Mechanical Engineering Department in Mustansiriyah University, Baghdad, Iraq.

References

Alizadeh, A., Bahadur, V., Zhong, S., Shang, W., Li, R., Ruud, J., Yamada, M., Ge, L., Dhinojwala, A., & Sohal, M. (2012). Temperature Dependent Droplet Impact Dynamics on Flat and Textured Surfaces. *Applied Physics Letters*, *100*(11), 111601.

Ashikhmin, A. E., Khomutov, N. A., Piskunov, M. V., & Yanovsky, V. A. (2020). Secondary Atomization of a Biodiesel Micro-Emulsion Fuel Droplet Colliding with a Heated Wall. *Applied Sciences*, *10*, 685.

Bielaczyc, P., Szczotka, A., & Woodburn, J. (2014). Cold Start Emissions of Spark-Ignition Engines at Low Ambient Temperatures as an Air Quality Risk. *Archives of Environmental Protection*, *40*(3), 86–100.

Borisov, A. A., Gel'fand, B. E., Natanzon, M. S., & Kossov, O. M. (1981). Droplet Breakup Regimes and Criteria for their Existence. *Journal of Engineering Physics*, *40*(1), 44–49.

Califano, V., Calabria, R., & Massoli, P. (2014). Experimental Evaluation of the Effect of Emulsion Stability on Micro-Explosion Phenomena for Water-in-Oil Emulsions. *Fuel*, *117*, 87–94.

Castanet, G., Dunand, P., Caballina, O., & Lemoine, F. (2013). High-Speed Shadow Imagery to Characterize the Size and Velocity of the Secondary Droplets Produced by Drop Impacts onto a Heated Surface. In *Experiments in Fluids* (Vol. 54, Issue 3).

Cen, C., Wu, H., Lee, C., Fan, L., & Liu, F. (2019). Experimental Investigation on the Sputtering and Micro-Explosion of Emulsion Fuel Droplets during Impact on a Heated Surface. *International Journal of Heat and Mass Transfer*, *132*, 130–137.

Chakaneh, J. Z., Javid, S. M., & Passandideh-Fard, M. (2019). Surface Roughness Effect on Droplet Impact Characterization: Experimental and Theoretical Study. *Journal of Mechanical Engineering and Sciences*, *13*(2), 5104–5125.

Crookes, R. J., Kiannejad, F., & Nazha, M. A. A. (1997). Systematic Assessment of Combustion Characteristics of Biofuels and Emulsions with Water for Use as Diesel Engine Fuels. *Energy Conversion and Management*, *38*(15–17), 1785–1795.

Dunand, P., Castanet, G., Gradeck, M., Maillet, D., & Lemoine, F. (2013). Energy Balance of Droplets Impinging onto a Wall Heated above the Leidenfrost Temperature. *International Journal of Heat and Fluid Flow*, *44*, 170–180.

Faik, A. M. D. (2017). *Quantitative Investigation of the Multicomponent Fuel Droplet Combustion Using High Speed Imaging and Digital Image Processing* (Issue August). The University of Sheffield.

Faik, A. M. D., & Zhang, Y. (2018). Multicomponent Fuel Droplet Combustion Investigation using Magnified High Speed Backlighting and Shadowgraph Imaging. *Fuel*, *221*(December 2017), 89–109.

Faik, A. M. E.-D., & Zhang, Y. (2020). Liquid-Phase Dynamics during the Two-Droplet Combustion of Diesel-Based Fuel Mixtures. *Experimental Thermal and Fluid Science*, *115*, 110084.

Faik, A. M. E. (2018). The Effect of Diesel-Alcohol Blends on The Cold-Start Combustion of a Compression Ignition Engine. *Journal of Engineering and Sustainable Development*, *22*(02), 20–29.

Gayatri, P., Das, P. K., & Manna, I. (2015). Droplet Oscillation and Pattern Formation during Leidenfrost Phenomenon. *Experimental Thermal and Fluid Science*, *60*, 346–353.

Ithnin, A. M., Ahmad, M. A., Bakar, M. A. A., Rajoo, S., & Yahya, W. J. (2015). Combustion Performance and Emission Analysis of Diesel Engine Fuelled with Water-in-Diesel Emulsion Fuel Made from Low-Grade Diesel Fuel. *Energy Conversion and Management*, *90*, 375–382.

Jackson, G. S., & Avedisian, C. T. (1998). Combustion of Unsupported Water-in-n-Heptane Emulsion Droplets in a Convection-Free Environment. *International Journal of Heat and Mass Transfer*, *41*(16), 2503–2515.

Jin, Z., Sui, D., & Yang, Z. (2015). The Impact, Freezing, and Melting Processes of a Water Droplet on an Inclined Cold Surface. In *International Journal of Heat and Mass Transfer* (Vol. 90, pp. 439–453).

Jin, Z., Zhang, H., & Yang, Z. (2016). The Impact and Freezing Processes of a Water Droplet on a Cold Surface with Different Inclined Angles. *International Journal of Heat and Mass Transfer*, *103*, 886–893.

Jowkar, S., & Morad, M. R. (2019). Rebounding Suppression of Droplet Impact on Hot Surfaces: Effect of Surface Temperature and Concaveness. In *Soft Matter* (Vol. 15, Issue 5, pp. 1017–1026).

Leal-Calderon, F., Schmitt, V., & Bibette, J. (2007). *Emulsion Science Basic Principles* (2nd Editio). Springer.

Li, D., & Duan, X. (2019). Numerical Analysis of Droplet Impact and Heat Transfer on an Inclined Wet Surface. *International Journal of Heat and Mass Transfer*, *128*, 459–468.

Li, H., Waldman, R. M., Zhang, K., & Hu, H. (2017). Quantification of Dynamic Water Droplet Impact onto a Solid Surface by using a Digital Image Projection Technique. In *AIAA SciTech Forum - 55th AIAA Aerospace Sciences Meeting*.

Mollet, H., & Grubenmann, A. (2001). *Formulation Technology: Emulsions, Suspensions, Solid Forms*. Wiley-VCH.

Moon, J. H., Cho, M., & Lee, S. H. (2016). Dynamic Wetting and Heat Transfer Characteristics of a Liquid Droplet Impinging on Heated Textured Surfaces. *International Journal of Heat and Mass Transfer*, *97*, 308–317.

Pulkrabek, W. W. (1997). *Engineering Fundamentals of the Internal Combustion Engine*. Prentice Hall.

Qi, W., & Weisensee, P. B. (2020). Dynamic Wetting and Heat Transfer during Droplet Impact on Bi-phobic Wettability-Patterned Surfaces. In *Physics of Fluids* (Vol. 32, Issue 6).

Qiao, Y. M., & Chandra, S. (1996). Boiling of Droplets on a Hot Surface in Low Gravity. *International Journal of Heat and Mass Transfer*, *39*(7), 1379–1393.

Raman, K. A., Jaiman, R. K., Lee, T. S., & Low, H. T. (2016). Lattice Boltzmann Simulations of Droplet Impact onto Surfaces with Varying Wettabilities. In *International Journal of Heat and Mass Transfer* (Vol. 95, pp. 336–354).

Rueda Villegas, L., Tanguy, S., Castanet, G., Caballina, O., & Lemoine, F. (2017). Direct Numerical Simulation of the Impact of a Droplet onto a Hot Surface above the Leidenfrost Temperature. In *International Journal of Heat and Mass Transfer* (Vol. 104, pp. 1090–1109).

Samuel, R. A., & Valan, A. A. (2014). Prediction of Cold Start Hydrocarbon Emissions of Air Cooled Two Wheeler Spark Ignition Engines by Simple Fuzzy Logic Simulation. *Thermal Science*, *18*(1), 179–191.

Sen, U., Roy, T., Ganguly, R., Angeloni, L. A., Schroeder, W. A., & Megaridis, C. M. (2020). Explosive Behavior during Binary-Droplet Impact on Superheated Substrates. *International Journal of Heat and Mass Transfer*, *154*, 119658.

Shi, Z., Lee, C., Wu, H., Li, H., Wu, Y., Zhang, L., & Liu, F. (2019). Effect of Nozzle Diameter on Macroscopic Spray Behavior of Heavy-Duty Diesel Engine under Cold-Start Conditions. *Atomization and Sprays*, *29*(8), 741–762.

Tanaka, R., Matsumoto, S., Kaneko, A., & Abe, Y. (2011). The Effect of Rotation on Resonant Frequency of Interfacial Oscillation of a Droplet using Electrostatic Levitator. *Journal of Physics: Conference Series*, *327*, 012021.

Tanimoto, D., & Shinjo, J. (2019). Numerical Simulation of Secondary Atomization of an Emulsion Fuel Droplet due to Puffing: Dynamics of Wall Interaction of a Sessile Droplet and Comparison with a Free Droplet. *Fuel*, *252*, 475–487.

Vellaiyan, S., Amirthagadeswaran, K. S. (2016). The Role of

Water-in-Diesel Emulsion and its Additives on Diesel Engine Performance and Emission Levels: A Retrospective Review. *Alexandria Engineering Journal*, *55*(3), 2463–2472.

Wamankar, A. K., Satapathy, A. K., & Murugan, S. (2015). Experimental Investigation of the Effect of Compression Ratio, Injection Timing & Pressure in a DI (Direct Injection) Diesel Engine Running on Carbon Black-Water-Diesel Emulsion. *Energy*, *93*, 511–520.

Wang, L., Zhang, R., Zhang, X., & Hao, P. (2017). Numerical Simulation of Droplet Impact on Textured Surfaces in a Hybrid State. *Microfluid Nanofluid*, *21*(61).

Wang, Z., Li, Y., Wang, C., Xu, H., & Wyszynski, M. L. (2016). Near-Nozzle Microscopic Characterization of Diesel Spray under Cold Start Conditions with Split Injection Strategy. *Fuel*, *181*, 366–375.

Yang, Z., Liu, F., & Li, Y. (2020). Autoignition Characteristics of Diesel Spray under Different Injection Pressures and Cold Start Strategy for Compression Ignition Engines. *International Journal of Engine Research*.

Zhang, R., Hao, P., Zhang, X., & He, F. (2018). Supercooled Water Droplet Impact on Superhydrophobic Surfaces with Various Roughness and Temperature. *International Journal of Heat and Mass Transfer*, *122*, 395–402.